Principal Static Wind Loads

N. Blaise[1] and V. Denoël[1]

[1]Structural Engineering Division, Faculty of Applied Sciences, University of Liège, Liège, Belgium. *N.Blaise@ulg.ac.be*

Abstract

The concept of static wind load is widely used in practice for structural wind design. In this context, this paper assesses the envelope reconstruction problem stated as follows: find the best set of static loadings that is optimum to reproduce by static analyses, the envelope values of structural responses resulting from a formal buffeting dynamic analysis. A solution was recently derived by means of Principal Static Wind Loads which are well-suited for this problem. The concept is illustrated with a large stadium roof and the accuracy of the envelope reconstruction is analysed.

1 Introduction

This paper illustrates a new type of loadings, the Principal Static Wind Loads (PSWLs), recently introduced by Blaise & Denoël (2013). These static loadings are well-suited for combinations (Blaise *et al.*, 2012) and are expected to reproduce by static analyses the envelope values, minimum and maximum, of internal forces resulting from a dynamic buffeting analysis. This *envelope reconstruction problem (Blaise & Denoël, 2013)* has already been tackled using different bases of static wind loads established with (i) Covariance Proper Transformation (CPT) (Katsumura *et al.*, 2007) or (ii) Spectral Proper Transformation (Fiore & Monaco, 2009) of the wind pressure field and (iii) Equivalent Static Wind Loads (ESWL) (Zhou *et al.*, 2011). Each of the aforementioned methods considers laborious combinations of their static wind loads in order to target all (i) or a selected number of (ii,iii) the envelope values. Unfortunately, the first two focus on the aerodynamic loading and therefore do not include the structural behaviour of the structure.

In this paper, we seek to demonstrate the optimality of the PSWL basis for combinations considering the envelope reconstruction problem. This is illustrated on "Le Grand Stade de Lille Métropole" which is a large stadium roof at Lille, France. The efficiency of the PSWL basis is assessed by comparison with CPT loading modes and ESWLs.

Figure 1-(a) shows three different parts of the roof: the retractable one and parts above the ambulatories and above the grandstands. Figure 1-(b) shows the standard deviations of the vertical external forces on the roof for a wind blowing from East and adequately derived from the aerodynamic pressures obtained with wind tunnel measurements on the model of the stadium shown in Fig. 1-(c).

2 Formal buffeting dynamic analysis

The aerodynamic pressures $\mathbf{q}_{tot}(t)$ obtained with wind-tunnel measurements, are transformed to nodal external forces $\mathbf{f}_{tot}(t)$ separated into a mean part $\boldsymbol{\mu}_p$ and a fluctuating part $\mathbf{f}(t)$

$$\mathbf{f}_{tot} = \boldsymbol{\mu}_f + \mathbf{f}.$$

The dynamic motion of the structure $\mathbf{x}$ is obtained by solving the equation of motion

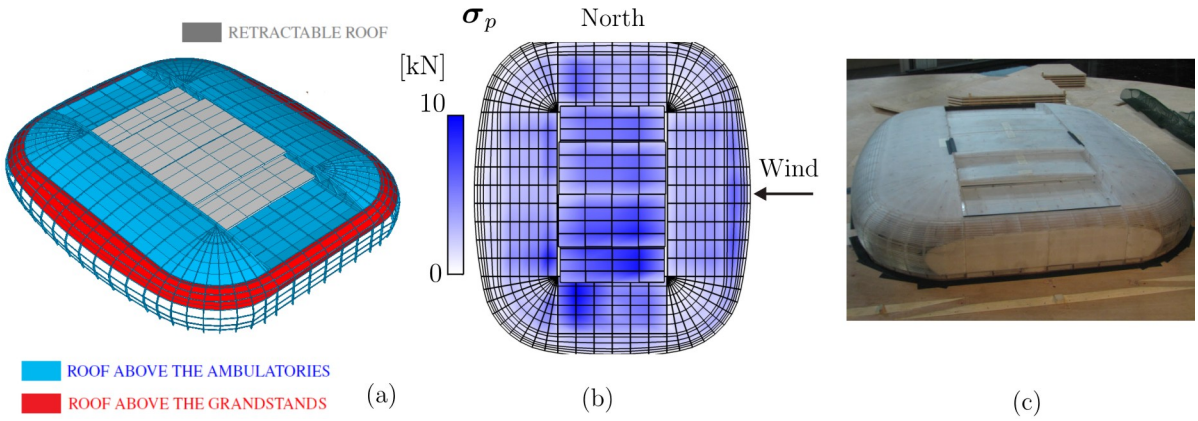

Figure 1: (a) Three different parts of the roof, (b) standard deviations of the vertical external forces on the roof for a wind blowing from east and (c) model of the stadium in the wind tunnel (courtesy of CSTB).

$$\mathbf{M}\ddot{\mathbf{x}} + \mathbf{C}\dot{\mathbf{x}} + \mathbf{K}\mathbf{x} = \mathbf{f}. \tag{1}$$

The mean part $\boldsymbol{\mu}_x$ and the background contribution $\mathbf{x}^{(\mathrm{B})}(t)$ of the nodal displacements are respectively obtained as

$$\boldsymbol{\mu}_x = \mathbf{K}^{-1}\boldsymbol{\mu}_f \quad ; \quad \mathbf{x}^{(\mathrm{B})} = \mathbf{K}^{-1}\mathbf{f}.$$

Because it is more appropriate, the resonant behaviour of the structure is computed by solving Eqn.1 in the modal basis

$$\mathbf{M}^\star\ddot{\boldsymbol{\eta}} + \mathbf{C}^\star\dot{\boldsymbol{\eta}} + \mathbf{K}^\star\boldsymbol{\eta} = \mathbf{f}^\star \qquad \boldsymbol{\eta}^{(\mathrm{R})} = \boldsymbol{\eta} - \mathbf{K}^{\star-1}\mathbf{f}^\star(t)$$

where $\mathbf{M}^\star$, $\mathbf{C}^\star$ and $\mathbf{K}^\star$ are the generalized mass, damping, and stiffness matrices respectively, $\boldsymbol{\eta}(t)$ are the modal coordinates, with $\boldsymbol{\eta}^{(\mathrm{R})}(t)$ their resonant contribution, $\mathbf{f}^\star(t)$ is the generalized forces and the dot denotes time derivative.

The total motion of the structure is expressed by

$$\mathbf{x}_{tot} = \boldsymbol{\mu}_x + \mathbf{x}^{(\mathrm{B})} + \boldsymbol{\phi}\boldsymbol{\eta}^{(\mathrm{R})}$$

where $\boldsymbol{\phi}$ collects the mode shapes. Results of the formal buffeting analysis can be found in (Blaise, 2011). Many structural responses —internal forces, reactions, stresses— are obtained by linear combinations of the nodal displacements

$$\mathbf{r}_{tot} = \mathbf{O}\,\mathbf{x}_{tot}$$

where $\mathbf{O}$ is a matrix of influence coefficients. For the design purpose, minimum $\mathbf{r}^{min}$ and maximum $\mathbf{r}^{max}$ values of structural responses may be computed as

$$\mathbf{r}^{min} = -g\boldsymbol{\sigma}_r \quad ; \quad \mathbf{r}^{max} = g\boldsymbol{\sigma}_r \tag{2}$$

where g is the unique peak factor (taken equal to 3.5 here for simplicity) and $\boldsymbol{\sigma}_r$ collects the standard deviations of the structural responses. Eqn.2 defines the envelope ($\mathbf{r}^{min}$, $\mathbf{r}^{max}$) and design of the structure is based on the design envelope ($\mathbf{r}^{d,min}$, $\mathbf{r}^{d,max}$) obtained by

$$\mathbf{r}^{d,min} = \boldsymbol{\mu}_r + \mathbf{r}^{min} \qquad ; \qquad \mathbf{r}^{d,max} = \boldsymbol{\mu}_r + \mathbf{r}^{max}$$

where $\boldsymbol{\mu}_r = \mathbf{O}\boldsymbol{\mu}_x$ is the mean part of the structural responses.

3 Envelope reconstruction problem

The problem tackled in this paper is the reconstruction of the envelope ($\mathbf{r}^{min}$, $\mathbf{r}^{max}$) obtained with the buffeting analysis detailed in Section 2 by means of static analyses under an appropriate set of static loadings $\mathbf{P}^s$ which we refer to with symbol s. The envelope that we want to reconstruct is composed of the six internal forces (axial force, two bending moments, two shear forces and torque) for all the beam elements (2542), giving $N^r = 30504$ structural responses.

Three sets of static loadings are established. They are composed of (i) loading modes obtained with covariance proper transformation (CPT) of the pressure field $(s \equiv c)$, (ii) equivalent static wind loads $(s \equiv e)$ and (iii) principal static wind loads $(s \equiv p)$.
(i) The CPT is applied to the covariance matrix of external forces $\mathbf{C}^f$

$$\left(\mathbf{C}^f - \mathbf{C}^c\mathbf{I}\right)\mathbf{P}^c = 0 \tag{3}$$

where $\mathbf{C}^c$ is a diagonal covariance matrix of principal components ordered by decreasing variances, $\mathbf{I}$ is the identity matrix and $\mathbf{P}^c$ collects the CPT loading modes.
(ii) Equivalent static wind loads $\mathbf{p}^e$ for each structural response that constitutes the envelope are first computed using the method in (Chen & Kareem, 2001) and then collected in a matrix $\mathbf{P}^e$.
(iii) The principal static wind load basis $\mathbf{P}^p$ is obtained by Singular Value Decomposition (SVD) of this matrix $\mathbf{P}^e$

$$\mathbf{P}^e = \mathbf{P}^p\mathbf{S}\mathbf{V}'.$$

With the SVD operation, each PSWL is no longer associated with a specific structural response, but rather aims at a global reconstruction of the set of equivalent static wind loads and, as a corollary, of the envelope of structural responses. Also, the PSWLs are well-suited for combinations because they are orthogonal vectors due to the SVD operation.

Each loading mode $\mathbf{p}_j^s$ produces a corresponding static response $\mathbf{r}_j^s$

$$\mathbf{r}_j^s = \mathbf{A}\mathbf{p}_j^s \qquad ; \qquad \mathbf{R}^s = \mathbf{A}\mathbf{P}^s$$

where $\mathbf{A}$=$\mathbf{O}\mathbf{K}^{-1}$ is a matrix of influence coefficients. Each static response is normalized such that $\mathbf{r}_j^s$ is somewhere tangent to the envelope.

The reconstruction of the envelope $\tilde{\mathbf{r}}_k^s = \left(\tilde{\mathbf{r}}_k^{s,min}, \tilde{\mathbf{r}}_k^{s,max}\right)$ after considering k loading modes is expressed by the recursive equations

$$\tilde{\mathbf{r}}_k^{s,min} = \min\left(\tilde{\mathbf{r}}_{(k-1)}^{s,min}; -\mathbf{r}_i^s; \mathbf{r}_i^s; \mathbf{0}\right) \qquad ; \qquad \tilde{\mathbf{r}}_k^{s,max} = \max\left(\tilde{\mathbf{r}}_{(k-1)}^{s,max}; -\mathbf{r}_i^s; \mathbf{r}_i^s; \mathbf{0}\right). \tag{4}$$

Notice that with Eqn.(4), $2k$ load cases are associated with the k^{th} reconstructed envelope. The envelope reconstruction accuracy is assessed by computing the relative errors defined as

$$\boldsymbol{\epsilon}_k = \frac{\tilde{\mathbf{r}}_k^{max} - \mathbf{r}^{max}}{\mathbf{r}^{max}} = \frac{\tilde{\mathbf{r}}_k^{min} - \mathbf{r}^{min}}{\mathbf{r}^{min}}.$$

where division is performed element by element.

For design purposes, a finite number of representative design load cases has to be selected. The ordering in the available set of loading modes is done based on the maximization of a choosen indicator of convergence. Such indicator of convergence is defined as the mean error of all structural responses:

$$\Psi_k = \frac{1}{N^r} \sum_{l}^{N^r} \epsilon_{lk} \tag{5}$$

where ϵ_{lk} is the relative error on the l^{th} structural response in the reconstructed envelope with k loading modes.

4 Illustration

The envelope reconstruction is first illustrated with 66 beam elements identified in bold in Fig. 2-(a). Also, the first ten elements selected for their ESWLs are identified in red. Figure 2-(b) depicts the real envelope of the axial forces for the 66 beam elements. Figure 2-(c) shows the ordering of the first fifty of the CPT loading modes and PSWLs.

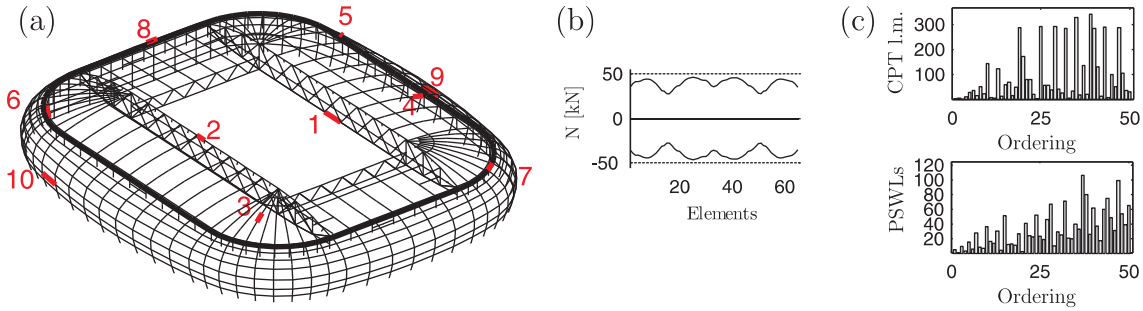

Figure 2: (a) Identification of the 66 beam elements considered for the illustration (in bold) and first ten elements selected with the indicator of convergence for the ESWLs basis (in red), (b) axial force envelope for the 66 beam elements and (c) ordering of the first fifty of the loading modes (CPTs and PSWLs) selected with the indicator of convergence.

4.1 Loading modes

Figure 3 shows, for the three sets of static loadings, the first, second, fifth and fiftieth loading modes (upper part of each graph), the corresponding static responses $\mathbf{r}_k^s$ and the sequential reconstruction of the envelope $\tilde{\mathbf{r}}_k^s$ (lower part of each graph) considering the first one, two, five and fifty loading modes (without combinations).

The first CPT loading mode loads the retractable roof and the Northern part with an asymmetric loading while the first ESWL mainly loads the retractable roof. The first PSWL produces a more complicated loading shape with asymmetric loadings on several parts of the roof. The first three have in common the loading of the windward part of the roof. The second CPT loading mode loads the leeward part of the roof and the second ESWL loads the leeward and retractable part with asymmetric loadings. The second PSWL heavily loads the south part of the retractable roof while the fifth ESWL loads the north part of the retractable roof. Instead of global loading on the roof, loading modes with increasing order produce local loadings as shown with the fiftieth loading modes.

Figure 3 also shows the relative errors for ten ranges of 5084 axial forces considering the first five and fifty loading modes for the sequential reconstruction of the envelope.

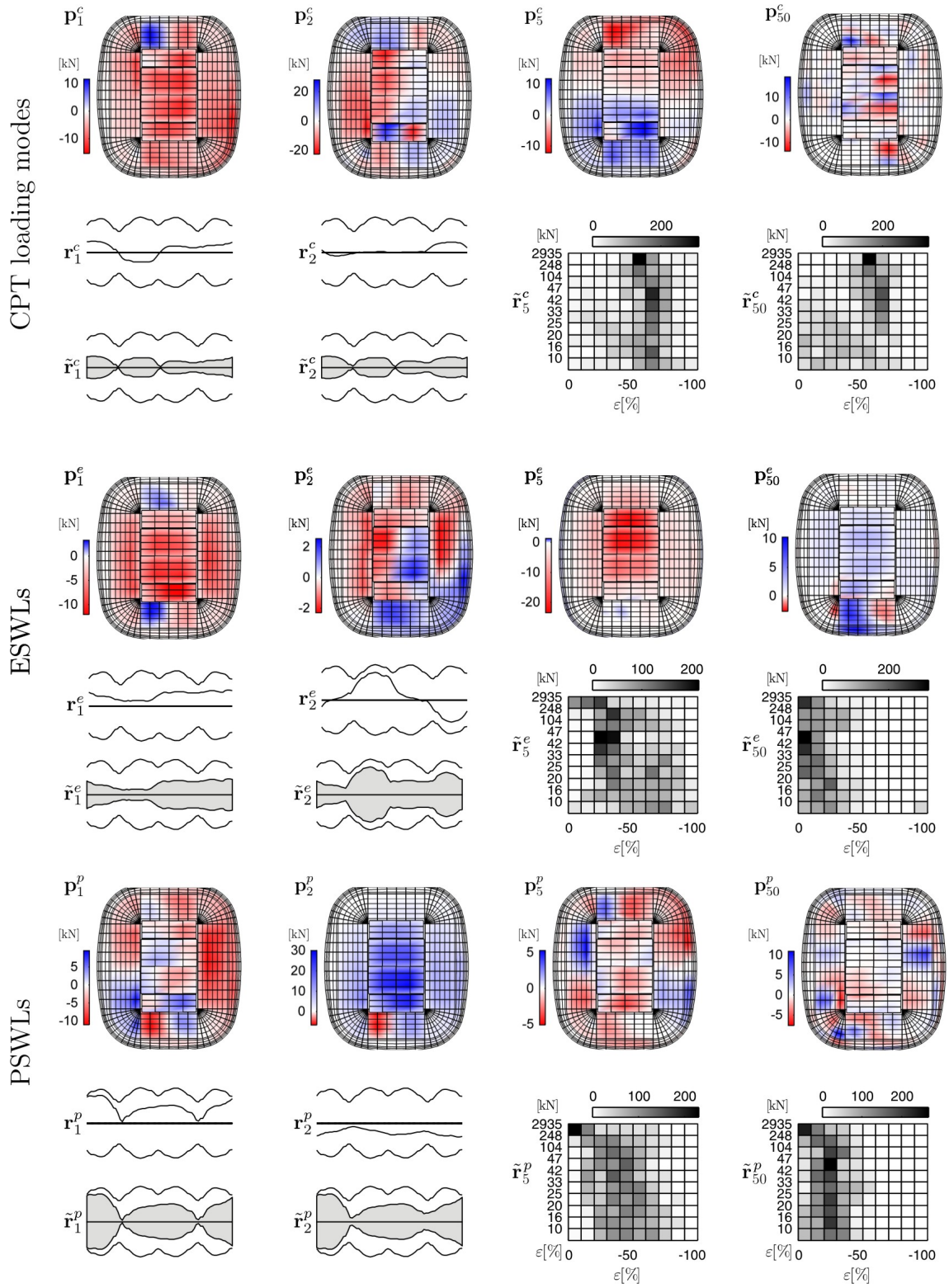

Figure 3: For each set of static loadings, the loading modes (upper part of each graph), the static responses $\mathbf{r}_k^s$ and the reconstructed envelope $\tilde{\mathbf{r}}_k^s$ (lower part of each graph).

With the first five or fifty CPT loading modes, each axial force is poorly reconstructed with a large

part that has a relative error larger than 50% in magnitude.

Application of the first five and fifty ESWLs improve significantly the reconstruction and most of the axial forces have underestimations in $[-50\%, 0]$, and $[-20\%, 0]$, respectively. Application of the first five PSWLs improves significantly the reconstruction, especially for large values of axial forces. The first fifty PSWL produces underestimations larger than $[-30\%, 0]$.

Due to the SVD operation, for the CPT loading modes and for the PSWLs, considering more loadings than fifty does not improve significantly the reconstructed envelope because no combination is considered. An interesting approach may be to consider combinations of them to ensure a higher rate of envelope reconstruction.

4.2 Combinations

Any arbitrary combination coefficients denoted by $\mathbf{q}^s$ of the CPT loading modes, ESWLs or PSWLs produces a new static loading denoted by $\mathbf{p}^{c_s} = \mathbf{P}^s\mathbf{q}^s$ associated with structural responses $\mathbf{r}^{c_s} = \mathbf{A}\mathbf{p}^{c_s}$.

The successive static analyses under each combination of the loadings modes, selected using the indicator of convergence, produce a sequential reconstruction of the envelope $\tilde{\mathbf{r}}_k^{c_s} = \left(\tilde{\mathbf{r}}_k^{c_s,min}, \tilde{\mathbf{r}}_k^{c_s,max}\right)$.

From a practical view point and with M loading modes, the combination coefficient are obtained by shooting in a random direction $(q_1^s, q_2^s, \ldots, q_M^s)$ generated with a Monte Carlo simulation technique ($10^{(M-1)}2^M$ generations), then by scaling the generated combination in order to restore the tangency condition with the actual envelope.

The combination coefficients of the first two, three and five loading modes are first generated with Monte-Carlo simulations. With the increase of the number of loadings M, Monte-Carlo simulation may become heavy to perform, considered combinations are predefined for the first six and ten loading modes. These predefined combinations are obtained by considering all possible combinations if each combination coefficient can take - 1,1 or 0 values scaled to fulfill the tangency condition. For M loadings, the subspace of considered combinations counts 3^{M-1} different couple of coefficients.

Figure 4 allows to appreciate the gain of reconstructed envelope accuracy by combinations of the loading modes. The evolution of Ψ is depicted as a function of the number of design wind loads derived with an increasing number of loading modes with or without combinations. The first three graphs from left to right are the results if no combination is considered and each loading mode is sequentially applied and if coefficients of Monte-Carlo simulation are used to combine the first two and three loading modes, respectively. The fourth, fifth and sixth graphs from left to right are the results if coefficients of Monte-Carlo simulation are used to combine the first five loading modes and if predefined considered combinations are used to combine the first six and ten loading modes, respectively.

Horizontal lines indicate the limit values for Ψ that would be obtained if all coefficients in the defined subspace of coefficients in the two approaches (coefficients of Monte-Carlo simulation or predefined considered combinations) were considered.

Figure 4 confirms that the ESWLs or PSWLs performed better than the CPT loading modes which are not suited for the envelope reconstruction because the behaviour of the structure is not incorporated. Without combinations, the PSWLs perform better than the ESWLs up to the 12 loading mode (24 design wind load) as a consequence of the SVD operation for the PSWLs. Indeed, the SVD operation produces an ordering with the principal coordinates and consideration of more and more PSWLs (or CPT loading modes) does not bring significant improvement of Ψ. With combinations of a reduced number of loading modes, the key-idea is to reach and even exceed the lower limit of the grey area fixed by the value of Ψ obtained with the first fifty ESWLs applied without combinations.

If combinations are considered, a rapid increase is observed with just the first few design wind loads, then followed by a transition zone where the slopes decrease with a slow monotonic convergence toward their respective limit values.

With combinations of the first four PSWLs, the grey area is not reached. More loading modes have to be combined and predefined considered combinations are considered. Considered combinations of the first six loading modes shows higher curves than the ones obtained with coefficients of Monte-Carlo simulation of the first four loading modes.

Considered combinations of the first ten PSWLs, allows to reach the grey area with a number of design wind loads divided by two and for 100 design wind loads, Ψ is equal to 12% in magnitude.

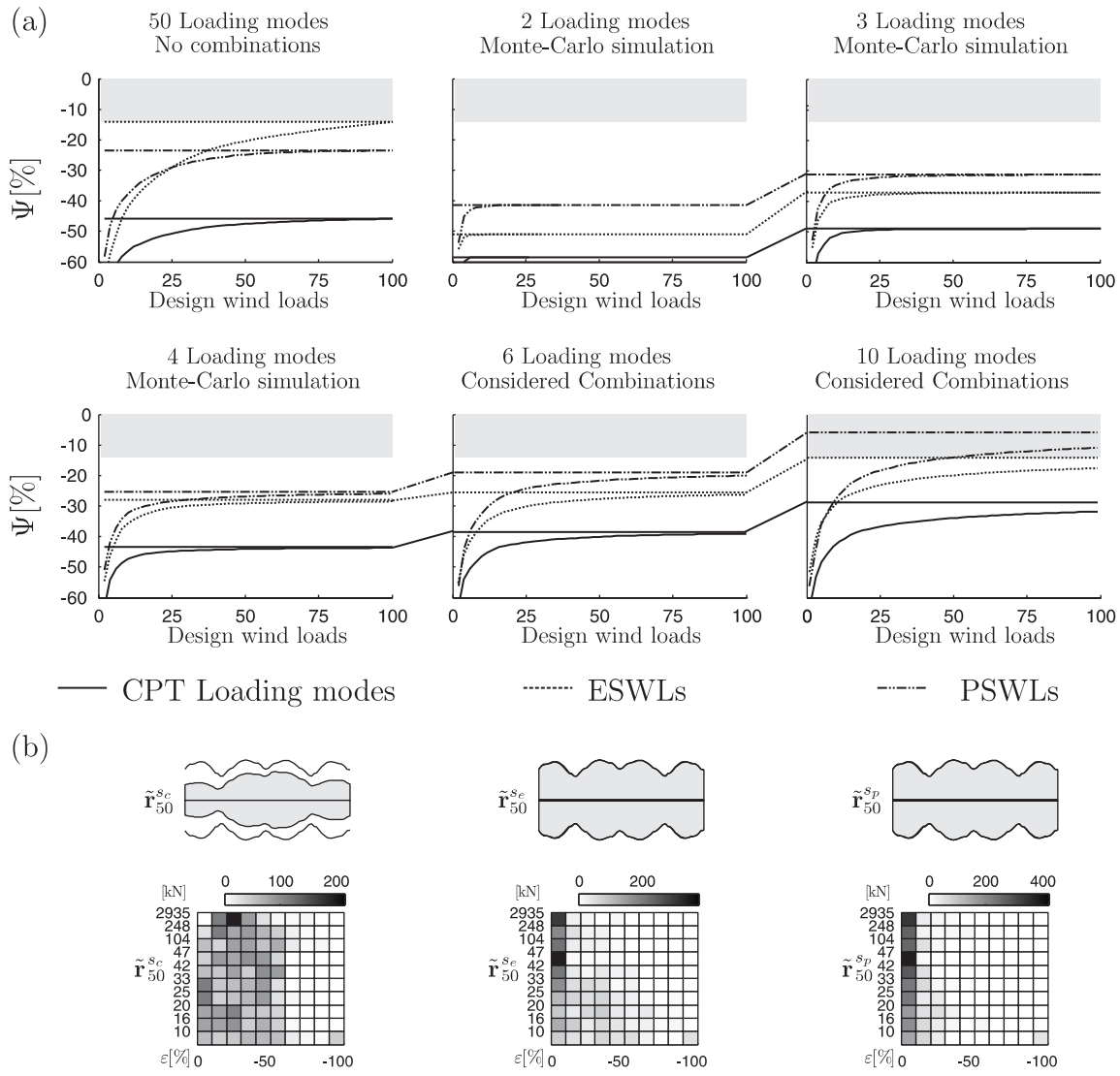

Figure 4: (a) Evolution of the indicator of convergence as a function of the subpaces considered for the coefficients and the number of CPT loading modes, ESWLs and PSWLs. Subpaces for the coefficients are without combinations, obtained with Monte-Carlo simulations and considered combinations. (b) Reconstructed envelope $\tilde{\mathbf{r}}_{50}^{c_s}$ for a basis composed of the first ten loading modes and considering 100 design wind loads.

Figure 4-(b) shows, for a basis composed of the first ten loading modes and considering 100 design

wind loads, the error on the reconstructed envelope of the 66 axial forces (upper part of each graph) and the distribution of the relative errors for ten ranges of 5084 axial forces (lower part of each graph) for (from left to right) the CPT loading modes, ESWLs and PSWLs.

5 Conclusion

A new type of wind loading, the principal static wind load, has been recently introduced as an optimum basis for the envelope reconstruction problem. Indeed, PSWLs are not associated with specific responses, contrary to the ESWLs, and include the structural behaviour of the structure, contrary to the CPT or SPT loading modes. Also combinations of them are not the result of a pseudo-inverse or a least-square optimization of a number of user-defined structural responses. Combinations of them aims at the maximization of a user-defined indicator of convergence considering all structural responses. Due to the SVD operation, PSWLs are well-suited for combinations and perform better than the CPT loadings modes or ESWLs for the envelope reconstruction problem. Moreover, only a reduced number of representative load patterns has to be kept.

Acknowledgement

We would like to acknowledge the "Centre Scientifique et Technique du Bâtiment" in Nantes in France and also the design office "Greisch" in Liège, in Belgium for having provided the measurements in wind tunnel and the finite element model, respectively.

References

Blaise, N., Denoël V. 2011. Stochastic analysis of a stadium roof from deterministic wind tunnel measurements. *In: Proceedings of 13th International Conference on Wind Engineering*.

Blaise, N., & Denoël, V. 2013. Principal Static Wind Loads. *Journal of Wind Engineering and Industrial Aerodynamics*, **113**, 29–39.

Blaise, N., Hamra, L., & Denoel, V. 2012. Principal Static Wind Loads on a large roof structure. *In: Proceedings of the 12th ANIV conference of wind engineering In Vento*. Proceedings of the 12th ANIV conference of wind engineering In Vento.

Chen, X. Z., & Kareem, A. 2001. Equivalent static wind loads for buffeting response of bridges. *Journal of Structural Engineering-Asce*, **127**(12), 1467–1475.

Fiore, A., & Monaco, P. 2009. POD-based representation of the alongwind equivalent static force for long-span bridges. *Wind and Structures, An International Journal*, **12**(3), 239–257.

Katsumura, A., Tamura, Y., & Nakamura, O. 2007. Universal wind load distribution simultaneously reproducing largest load effects in all subject members on large-span cantilevered roof. *Journal of Wind Engineering and Industrial Aerodynamics*, **95**(9-11), 1145–1165.

Zhou, X., Gu, M., & Li, G. 2011. Application Research of Constrained Least-Squares Method in Computing Equivalent Static Wind Loads. *In: Proceedings of the 13th International Conference on Wind Engineering*.